COMPARISON OF $LU_3AL_5O_{12}$:CE(ER) BULK AND NANO SINGLE CRYSTALS

David JOHN[1,2,3], Jakub VOLF[1], Karol BARTOSIEWICZ[1], Takahiko HORIAI[4], Kei KAMADA[4,5], Akira YOSHIKAWA[4,5,6], Zdeněk REMEŠ[1], Lucie LANDOVÁ[1], Gilles LEDOUX[7], Julien HOUEL[7], Andrey PROKHOROV[1,8], Maksym BURYI[8]

[1]*Institute of Physics of the Czech Academy of Sciences, Prague, Czech Republic, EU, john@fzu.cz*

[2]*Faculty of Nuclear Sciences and Physical Engineering, Czech Technical University, Prague, Czech Republic, EU*

[3]*Nuclear Physics Institute of the Czech Academy of Sciences, Prague, Czech Republic, EU*

[4]*New Industry Creation Hatchery Center, Tohoku University, 2-1-1 Katahira Aoba-ku, Sendai, Miyagi, Japan*

[5]*C&A Corporation, T-Biz, 6-6-10 Aoba, Aramaki, Aoba-ku, Sendai, Miyagi, Japan*

[6]*Institute for Materials Research, Tohoku University, 2-1-1 Katahira Aoba-ku, Sendai, Miyagi, Japan*

[7]*Institut Lumière Matière, UMR5306 Université Lyon 1-CNRS, Université de Lyon, Villeurbanne, France, EU*

[8]*Institute of Plasma Physics of the Czech Academy of Sciences, Prague, Czech Republic, EU*

https://doi.org/10.37904/nanocon.2025.4979

Abstract

Lutetium aluminum garnet (LuAG) is a crystal well known for being extraordinarily useful for building highly efficient laser devices or ionizing radiation detectors. To design the most favourable physical properties, different dopants and synthesis methods are constantly developed, primarily focused on the advantages of single crystals. However, the downscaling of the luminescent materials to nanosize also creates additional benefits of increased surface to volume ratio and thus, the efficiency of luminescence or doping can be improved. Therefore, the aim of this work is to compare the single crystals and nanogarnets under the influence of Ce and Er doping. Optical properties of the garnet single crystals are very well known while the nanocrystals should have been studied first. Synergy methods like X-ray diffraction (XRD), photoluminescence (PL), photothermal deflection spectroscopies (PDS) were applied to the LuAG:Ce(Er) nanocrystals whereas the electron paramagnetic resonance (EPR) measurements were carried out in both single and nanocrystals. The main conclusion is that cerium enters nanocrystalline lattice becoming Ce^{4+} compensated by the Cr^{2+}, Fe^{2+} ions (accidental impurities) whereas it is also Ce^{3+} in the single crystal. About one order of magnitude larger Er^{3+} content was observed in the case of nanocrystals as compared to single crystals.

Keywords: Lutetium aluminum garnet, Erbium, Cerium, Single crystal, Nanocrystal, Photoluminescence, EPR

1. INTRODUCTION

Lutetium aluminum garnet (LuAG, $Lu_3Al_5O_{12}$) is a crystalline material known for its exceptional physical properties. LuAG exhibits over the other rare-earth garnets its rich light yield, small lattice parameter, high density and stability combined with fast thermal conductivity, which makes it especially useful for building highly efficient laser devices or ionizing radiation detectors [1]. To design the most favorable physical properties, different dopants and synthesis methods are constantly developed [2], primarily focused on advantages of lanthanoid-doping single-crystals. LuAG has a complex cubic crystal structure based on the presence of lutetium ion. The lutetium is relatively close to other lanthanides which means that even high levels of doping can conserve its favorable physical properties. Most attention is directed to erbium and cerium because their application, e.g. Er wavelength is strongly absorbed by water fluids which makes it promising for medical laser applications, and Ce has fast luminescence emission in the range well suitable for photodiode. The cerium

doped isostructural aluminum garnets were studied [3]. Despite the isomorphism between LuAG and YAG, some different and major advantages of LuAG can be expected. For example, the interactions between crystal field and rare earth ions in case of lutetium are higher, which leads to the larger Stark splitting of the lower laser manifold of doped rare earth ions, lower thermal occupation of the lower laser level, and therefore to the improvement of emission efficiency [4]. In this work we focus on optical properties of Er or Ce doped LuAG, we also use the downscaling of the luminescent materials to nanosize which creates additional benefits of increased surface to volume ratio and a substantial increase in the proportion of point defects that can then be more easily investigated. Therefore, the X-ray diffraction (XRD), Raman, photoluminescence (PL) and photothermal deflection spectroscopies (PDS) were applied to the newly synthesized LuAG:Ce(Er) nanopowders, to compare results with classic spectra of their bulk single-crystal counterparts.

2. EXPERIMENTAL CONDITIONS

2.1 Samples preparation

Nanocrystalline garnets of composition $Lu_{3-y}X_yAl_5O_{12}$ (X = Ce, Er) with y = 0.3 were prepared using a sol-gel combustion technique. The starting chemicals were, Lu_2O_3 (4 N, Sigma-Aldrich), $Al(NO_3)_3{\cdot}9H_2O$ (4 N, Sigma-Aldrich), Er_2O_3 (4 N, Sigma-Aldrich) and CeO_2 (4 N, Sigma-Aldrich). These were weighed in a total batch of 1 g of the resulting products. The starting chemicals were then dissolved in HNO_3 (65+ wt%, p.a., PENTA) and the excess HNO_3 was subsequently removed at 90 °C. The dried metal nitrates were then dissolved in 50 mL of deionized water. The metal nitrates in water solution were chelated by addition of citric acid monohydrate (>99.5, Sigma-Aldrich), where the molar ratio of citric acid to all metal ions was 2.5:1. The pH of the stirred solution was then set to pH ~ 8 (at room temperature) by dropwise addition of NH_4OH (24+ wt%, p.a., PENTA). The stirred solution was heated at 90 °C overnight to obtain a homogeneous gel. The dried gel was decomposed in a furnace at 800 °C for 2 h and finally at 1000 ◦C for 1 h.

Single crystals of LuAG were grown using the micro-pulling down (μ-PD) method. Four crystal variants were prepared: pure LuAG and two doped compositions (LuAG:Ce 0.5%, and LuAG:Er 0.2%). The crystal growth was performed in a μ-PD system with a radio frequency (RF) generator at 26 kVA [5]. The growth process utilized an iridium crucible with a 20 mm diameter, fitted with a 3 mm die containing a 0.5 mm diameter capillary channel. The starting materials consisted of high-purity (4N) oxide powders of Lu_2O_3, Er_2O_3, Al_2O_3, and Ce_2O_3, all obtained from Iwatani Corporation. Following the powder mixing in appropriate stoichiometric ratios, the mixture was placed in the iridium crucible. The crystal growth was initiated on a LuAG seed crystal oriented in the <100> direction, with the entire process conducted in an argon atmosphere. A steady crystal pulling rate of 0.05 mm/min was maintained throughout the growth process.

2.2 Experimental techniques

For crystal structure analysis the powder X-ray diffractometer (Empyrean, Malvern Panalytical) with Cu $K_{<\alpha>}$ radiation (at U = 45 kV, I = 30 mA) was used. The X-Ray diffraction patterns were measured in the range of 2θ from 5 till 120 degrees with a step 0.013 degree and time per step 100 s. The characterization of powders was made in the Bragg-Brentano geometry using fixed divergence slit with anti-scatter slit, scanning line detector 1D, and Ni filter. To avoid the reflections from the sample holder powders were on the SiC single crystal wafer with the definite cut. The crystallite sizes were determined using Rietveld refinement method.

Photoluminescence spectroscopy UV-exited photoluminescence (PL) emission spectra were measured in the 375–750 nm spectral range using commercial pulsed UV light emitting diode (LED) #XSL-360-5E (Roither Lasertechnik, GmbH, Vienna, Austria, wavelength 360 nm, output power 1 mW) operating in ac mode, a narrow band pass optical filter BP360 (Thorlabs #FBH360-10 transparent in 350–370 nm spectra range), long pass optical filter LP375 (Edmund Optics #34-302 transparent above 375 nm), a monochromator (Horiba H20VIS, spectral range 300-800 nm, spectral resolution 4 nm), a red-sensitive photomultiplier (Photonis

#XP2203B, spectral range 300-750 nm) and a 50 MHz lock-in amplifier (Zurich Instruments HF2LI). Biased sine modulated power for the UV LED was provided directly by HF2LI via built-in sine-wave generator. PMT photocurrent was converted to voltage signal by current amplifier (Zurich Instruments HF2TA). The HF2LI allowed also to visualize the measured signal using build-in oscilloscope. The setup was spectrally calibrated with a calibrated halogen lamp (Oriel Instruments #63358).

Electron paramagnetic resonance (EPR) spectra of X-band (9.4 GHz) measurements were obtained using a commercial Bruker ELEXSYS E580 spectrometer cooling by liquid Helium.

Custom-made photothermal deflection spectroscope (PDS) consists of previous light source with focusing optics, monochromator and optical filters, mechanical chopper, beamspliter, Si + InGaAs detector, spherical mirror, HeNe probe laser, flat mirror, focusing lenses, position detector, sample immersed in liquid, and anti-vibration table.

The size and morphology of ZnO NRs has been checked by scanning electron microscopy (SEM) using MAIA3, TESCAN electron microscope with the in-beam SE detector placed in objective lens and the electron beam energy 5 keV.

3. RESULTS AND DISCUSSION

3.1 X-ray diffraction and scanning electron microscopy analysis

The microscopy images and XRD patterns of the LuAG nanocrystals samples are shown in **Figure 1**.

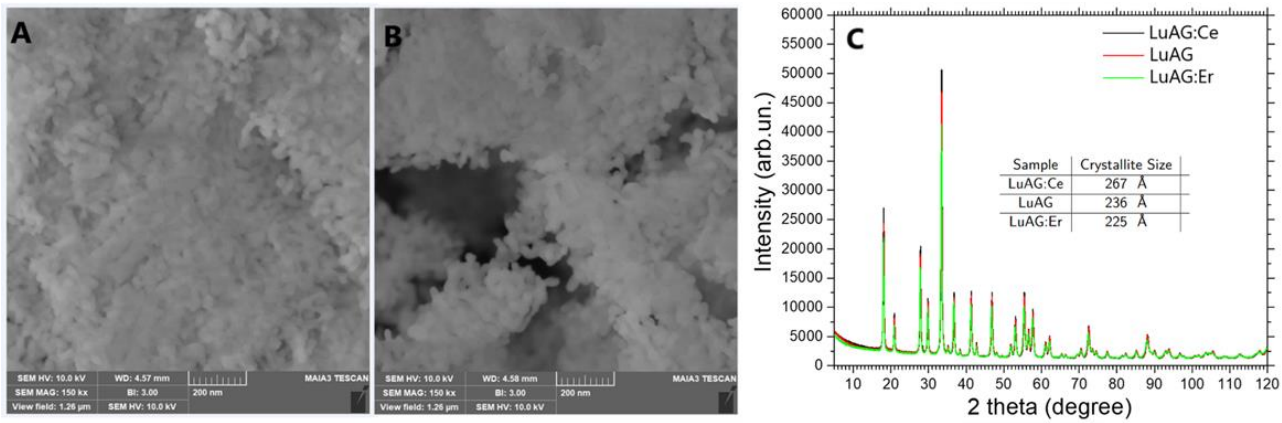

Figure 1 SEM images of the LuAG nanocrystals samples, undoped (A), doped by Ce (B), and XRD patterns of LuAG:Ce(Er) (C). Error of crystallite sizes determination (Rietveld method) was 10%.

From this follows that all samples have the same crystalline phase and very similar pattern, their crystal symmetry is cubic and space group Ia-3d. The crystallite size and micro strain were determined for all samples from exact value 2θ angles higher than 60 degrees. LuAG:Ce, LuAG, LuAG:Er have crystallite size 26.7, 23.6, 22.5 nm and micro strain 5.0197, 5.6643 and 5.949 nm, respectively (see also **Figure 1C**).

To have visual idea of the nanocystallites size, the SEM images of the samples were obtained and shown in **Figure 1A** and **1B**. Indeed, the average size of the nanocrystallites can be expected to be in the range of 20-30 nm. This correlates well with the XRD data.

3.2 Photoluminescence spectroscopy

The luminescence and optical absorption properties of the bulk single-crystal garnets are well known. Therefore, only the luminescence of nanocrystals has been considered in this paper. Two relatively weak peaks at 420 and 440 nm were detected in PL spectrum of all LuAG samples (**Figure 2**) with the same mean

decay time around 17 ns (this is evident from **Figure 2A, D** on example of undoped LuAG). These bands originate from surface contamination (the same signals have previously been observed in totally different samples, e.g. in SiO_2) with some organics, probably, the remaining precursors (see Experimental).

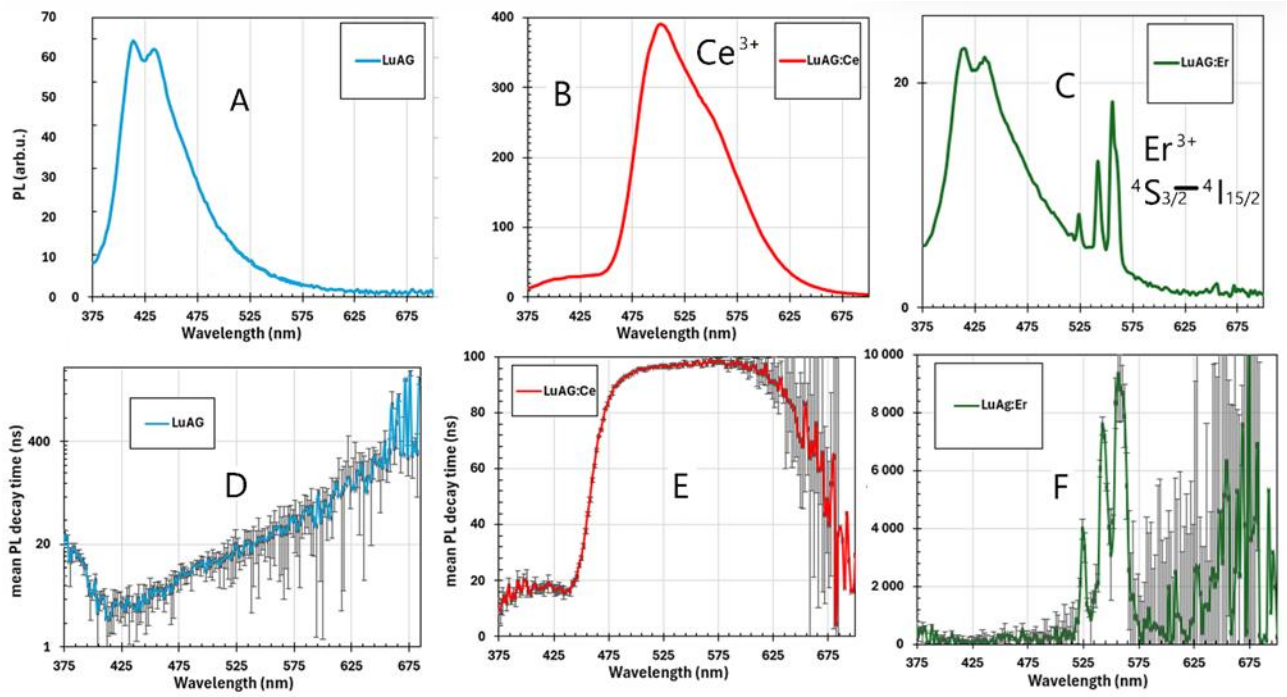

Figure 2 PL in visible range and its mean decay time spectra of the samples A,D) LuAG, B,E) LuAG:Ce and C,F) LuAG:Er, respectively

Otherwise, the pure LuAG generates no other clearly resolved emission bands in visible range (**Figure 2A**). The LuAG:Ce emits at 505 and 552 nm (**Figure 2B**). These are typical 5d - $^2F_{5/2}$ and 5d - $^2F_{7/2}$ transitions of Ce [6]. The energy levels scheme is shown in **Figure 3A**. However, at this point, it is hard to claim for sure which charge state of cerium (Ce^{3+} or Ce^{4+}) is responsible for them. This will be confirmed by EPR and PDS measurements below. The mean decay time measured is constant over the spectral range studied with the approximate value of 100 ns (**Figure 2E**). The LuAG:Er emission is characterized by 3 relatively strong and two very weak peaks in visible range at 524, 542, 556, 656 and 680 nm, respectively (**Figure 2C**). Some of these peaks can be linked to the energy level scheme of Er^{3+} (**Figure 3B**): 524 nm corresponds to $^2H_{11/2}$ -> $^4I_{15/2}$, 556 nm to $^4S_{3/2}$ -> $^4I_{15/2}$ and 654 nm to $^4S_{9/2}$ -> $^4I_{15/2}$ transitions. The mean decay time of the first three peaks is 4, 8, 9 µs, respectively (**Figure 2F**). As for the other two peaks – due to their weak intensity the mean decay time could only be roughly estimated to be in the range 6-10 µs.

The nanoscale and increased surface to volume ratio resulted in no significant increase in photoluminescence range nor intensity as compared to the single crystals or ceramics [7]. To gain better insight into the luminescence properties of the LuAG samples, the IR PL has been measured there as well (**Figure 3C**). The spectra of undoped LuAG and LuAG:Ce were the same - very broad band covering the 1080-1680 nm range, (**Figure 3C** blue/red) overlapped with several small but sharp peaks (like 1623 and 1625 nm) at the ends of spectra.

The LuAG:Er spectra have at least 5 clearly visible peaks in infrared PL spectrum around 1460, 1530, 1580, 1620 and 1660 nm which corresponds to commonly known Er^{3+} transitions between Stark levels ($^4I_{13/2}$ to $^4I_{15/2}$). This indicates the Er incorporation into the LuAG host, especially considering the pure garnet phase confirmed by XRD above (**Figure 1**). The broad IR emission (covering the 1080-1680 nm range) in all the samples should

originate from Cr^{2+} [8] as the existence of Cr^{3+} has been proven by EPR below, therefore, one cannot exclude the existence of other charge states. The origin of the 1623 and 1625 nm peaks is unknown.

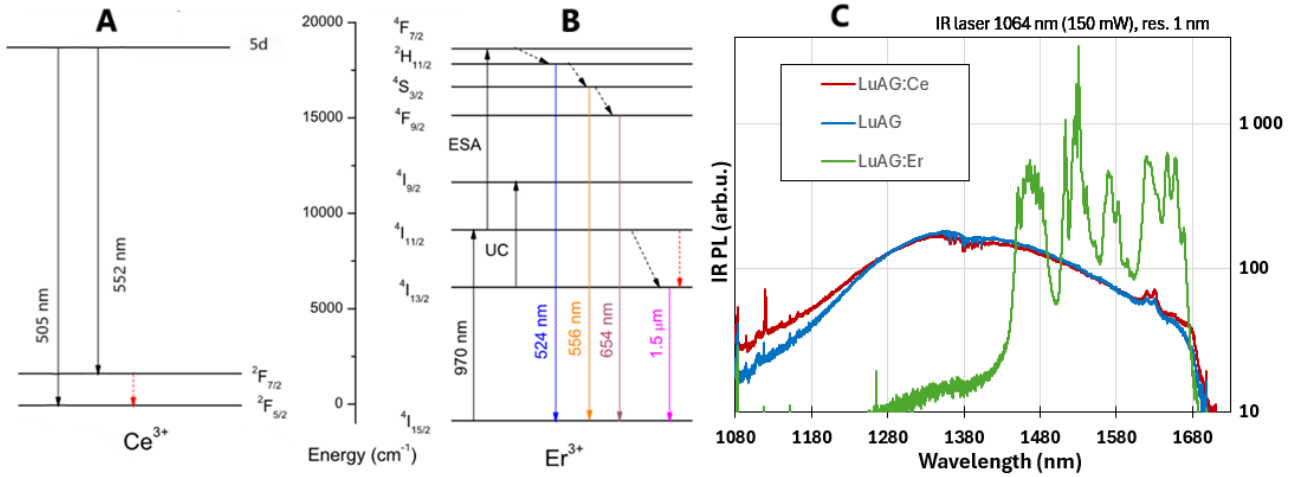

Figure 3 Energy levels scheme of Ce^{3+} (A) and Er^{3+} (B), and IR PL spectra of LuAG:Ce(Er) nanocrystals (C)

3.3 Defect states by photothermal deflection spectroscopy

PDS can be used to reveal more details about deep defect absorption states. The corresponding absorptance spectra are shown in **Figure 4**. All of them have clearly visible backgrounds. They are probably somehow correlated with the origin of the broad IR emission (covering the 1080-1680 nm range) in **Figure 4**. There are new bands starting to appear above 1275 nm in the LuAG:Ce(Er) whereas the absorptance is at the zero level in the case of the undoped LuAG. The origin of these new bands is unknown.

The effect of doping can be seen. Ce enhanced absorption in the region 275-375 nm. This is the typical Ce^{4+} charge transfer (CT) absorption in LuAG:Ce. Er^{3+} transitions are clearly detectable as well in LuAG:Er. The corresponding absorption bands are visible at around 475, 525, 655 and 970 nm, corresponding to the transitions $^4I_{15/2}$ to $^4F_{7/2}$, $^2F_{11/2}$, $^4F_{9/2}$ and $^4I_{11/2}$, respectively.

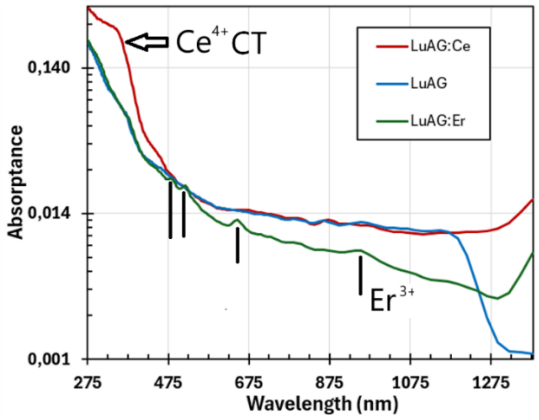

Figure 4 A) LuAG:(Ce,Er) absorptance measured by PDS. Ce^{4+} charge transfer and Er^{3+} specific transitions are indicated

3.4 Charge states and localization of point defects by EPR

To obtain more information about cerium and erbium as well as accidental impurities incorporation, electron paramagnetic resonance (EPR) was measured in all three samples. EPR spectra of the nanoparticles are shown in **Figure 5**.

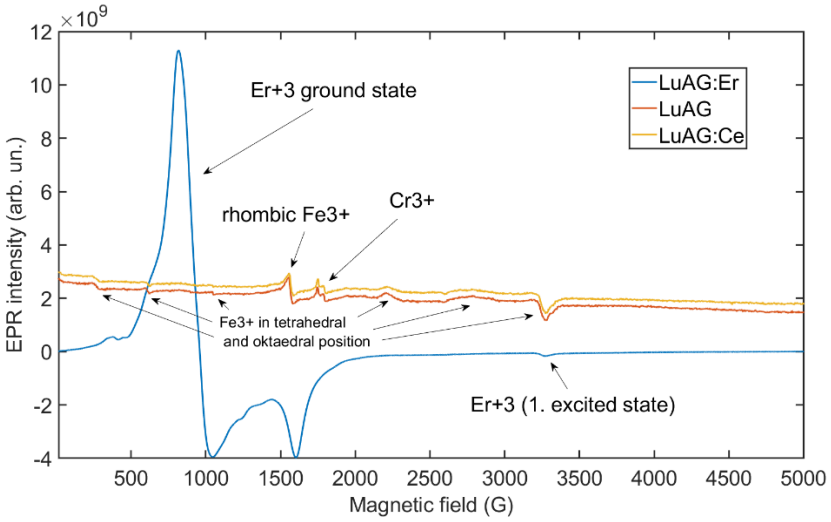

Figure 5 EPR spectra of LuAG:Ce(Er) nanocrystals measured under liquid nitrogen temperature, identified defects are marked with an arrow

EPR signal of Ce^{3+} is known to have very specific temperature dependence. Therefore, to detect its presence in the sample, the spectrum was measured stepwise lowering the temperature from 70 to 30 K. No resonances typical for Ce^{3+} were observed. The LuAG and LuAG:Ce surprisingly generated similar spectra. They were composed of the resonances typical for rhombic Fe^{3+}, Fe^{3+} octahedral and tetrahedral and Cr^{3+} [10]. This indicates only the Ce^{4+} existence (confirmed by PDS) in the LuAG:Ce and, therefore, the observed cerium PL is produced by Ce^{4+}. These results also correlate well with the existence of broad bands in the absorptance and infrared photoluminescence spectra. Er^{3+} signal is very strong and broad. Therefore, one may expect it to be incorporated instead of Lu. Moreover, the dominating is the signal produced by the ground. state, $^4I_{15/2}$, and very weak one produced by the $^4I_{13/2}$, first excited state.

EPR spectra were also measured in the powdered undoped LuAG and LuAG:Ce(Er) single crystals and shown in **Figure 6**. The spectrum of the undoped single crystal LuAG looks very similar to the one measured in the undoped and LuAG:Ce nanocrystalline powder. The typical transitions of the Cr^{3+} were revealed and their positions were indicated with the g factor values.

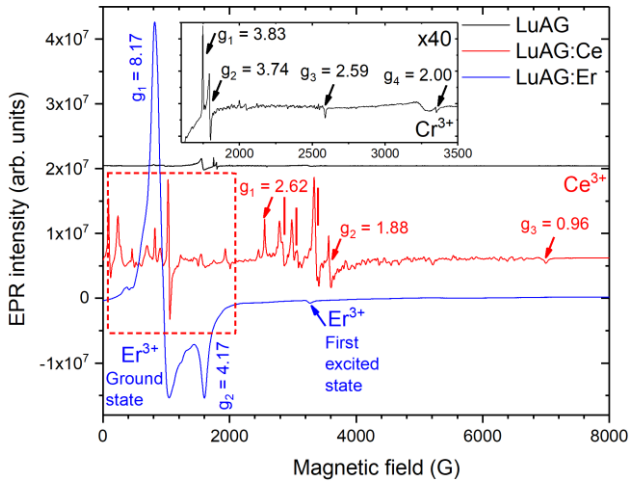

Figure 6 EPR spectra measured at T = 10 K in the powdered single crystals of undoped LuAG and LuAG:Ce(Er). Specific g_i factors indicate the positions of contributions of the specific ions in spectra. Resonances originating from ground and first excited states of Er^{3+} are stressed. Vertical bars and dashed oblong mark the resonances originating from octahedral and tetrahedral Fe^{3+}

The Ce^{3+} incorporation into the LuAG or YAG single crystal is very well known. The corresponding spectrum can be seen in **Figure 6**. Therefore, it is surprising that in the nanocrystals, the whole cerium appears as Ce^{4+}. This must have required additional charge compensation in the nanocrystals, e.g., Fe^{2+}, Cr^{2+} + Ce^{4+} this correlate well to the luminescence measurements. One may conclude that in the case of single crystals the iron (also detected, see **Figure 6**), chromium (mixed up with iron contributions in **Figure 6**) and cerium ions all are in the 3+ charge state and do not appear close to each other enough for the charge transformation to appear. In contrast, considering the size of the LuAG crystallites (about 20 nm, equal to the 3 lattice parameter values) in the case of the nanocrystals – the impurity transition ions appear close to cerium resulting in the charge transformation.

The Er^{3+} spectrum is just the same as in the case of nanocrystalline LuAG (**Figure 6**). The determined *g* factor values are shown in **Figure 6**. The intensity of the Er^{3+} spectrum is about one order of magnitude larger in the nanocrystals as compared to the single crystals (see **Figures 3, 6**). Considering Er doping levels (see Experimenrtal) one may conclude that the segregation coefficient must be larger in the single crystals. Taking into account that Er creates garnet phase as well, one may expect indeed easier tensions relaxation in the case of nanocrystals as compared to the single crystals when Er enters the LuAG lattice.

4. CONCLUSION

According to X-ray diffraction, the nanocrystals are pure phase cubic system of space group Ia-3d, pure phase LuAG:Ce, LuAG or LuAG:Er with homogeneous crystallite size 27, 24, 23 nm and micro strain 0.50197, 0.56643 and 0.5949 Å, respectively. The LuAG:Ce nanocrystals emits at 505 and 552 nm. These peaks are typical for Ce^{4+} (confirmed by the existence of the typical Ce^{4+} charge transfer absorption). LuAG:Er PL spectrum has 5 peaks of about 1460, 1530, 1580, 1620 and 1660 nm which are commonly known Er^{3+} transitions between Stark levels. The pure LuAG emits only negligible, however, the large surface area of nanoparticles traps contamination from the precursors used, which weakly emits at two peaks of 420 and 440 nm. In LuAG and LuAG:Ce infrared spectra very broad (1180 to 1680 nm) band of uncertain origin, probably Cr^{2+} is present. Chrom and iron are present as accidental impurities. They play a significant role in the Ce^{4+} stabilization in the LuAG nanocrystals. Erbium content is about one order of magnitude larger in the nanocrystals as compared to the single crystals. This is because of easier tensions release in the case of nanocrystals whereas in the single crystals this can be more complicated due to large volume resulting in the lowered flexibility of the lattice in contrast to the nanocrystals.

ACKNOWLEDGEMENTS

The financial support of the Leading Agency National Science Centre - Czech Science Foundation project No. 24-14580L is gratefully acknowledged. The work was also supported by Ministry of Education, Youth and Sports of Czech Republic (MEYS) Danube project 8X23025 and the program "Strategy AV 21" of the Czech Academy of Sciences, specifically work package VP 27 Sustainable Energy (Renewable energy resources and distributed energy systems).

REFERENCES

[1] CHEREPY, N. J.; KUNTZ, J. D.; TILLOTSON, T. M.; SPEAKS, D. T.; PAYNE, S. A.; CHAI, B. H. T.; PORTER-CHAPMAN, Y.; DERENZO, S. E. Cerium-doped single crystal and transparent ceramic lutetium aluminum garnet scintillators. *Nuclear Instruments and Methods in Physics Research Section a Accelerators Spectrometers Detectors and Associated Equipment.* 2007, vol. 579, no. 1, pp. 38–41. Available from: https://doi.org/10.1016/j.nima.2007.04.009.

[2] TRETYAK E.V., SHEVCHENKO G.P., KORJIK M.V. Formation of high-density scintillation ceramic from LuAG:Ce + Lu2O3 powders obtained by co-precipitation method. *Optical Materials*. 2015, vol. 46, pp. 596-600, Available from: https://10.1016/j.optmat.2015.05.036

[3] LI, J.; SAHI, S.; GROZA, M.; PAN, Y.; BURGER, A.; KENARANGUI, R.; CHEN, W. Optical and scintillation properties of CE3+-Doped LUAG and YAG Transparent ceramics: a comparative study. *Journal of the American Ceramic Society.* 2016, vol. 100, no. 1, pp. 150–156. Available from: https://doi.org/10.1111/jace.14461.

[4] PEIXIONG Z., ZHENQIANG C., YIN H., ZHEN L., HAO Y., SIQI Z., SHENHE F., ANMING L., Enhanced emission of the 1.50–1.67 μm fluorescence in Er3+, Ce3+–codoped Lu3Al5O12 crystal. *Journal of Alloys and Compounds*. 2017, vol. 696, pp. 795-798. ISSN 0925-8388. Available from: https://doi.org/10.1016/j.jallcom.2016.12.003.

[5] VEBER, P.; BARTOSIEWICZ, K.; DEBRAY, J.; ALOMBERT-GOGET, G.; BENAMARA, O.; MOTTO-ROS, V.; THI, M. P.; BORTA-BOYON, A.; CABANE, H.; LEBBOU, K.; LEVASSORT, F.; KAMADA, K.; YOSHIKAWA, A.; MAGLIONE, M. Lead-free piezoelectric crystals grown by the micro-pulling down technique in the BaTiO3–CaTiO3–BaZrO3 system. *CrystEngComm.* 2019, vol. *21,* no. 25, pp. 3844–3853. Available from: https://doi.org/10.1039/c9ce00405j.

[6] LI, H.-L.; LIU, X.-J.; HUANG, L.-P. Luminescent properties of LuAG:Ce phosphors with different Ce contents prepared by a sol–gel combustion method. *Optical Materials.* 2006, vol. *29,* no. 9, pp. 1138–1142. Available from: https://doi.org/10.1016/j.optmat.2006.05.002.

[7] KHANIN, V.; MEIJERINK, A.; HOUTEPEN, A. J.; JAGT, H. J. B.; DE BOER, D. K. G. Photosaturation in luminescent LUAG:CE Garnet Concentrator Rods. *Advanced Photonics Research.* 2021, vol. 2, no. 8. Available from: https://doi.org/10.1002/adpr.202100055.

[8] FEDOROV, V.; CARLSON, T.; MIROV, S. Energy transfer in iron-chromium co-doped ZnSe middle-infrared laser crystals. *Optical Materials Express.* 2019, vol. 9, no. 5, 2340. Available from: https://doi.org/10.1364/ome.9.002340